The Three-Transponder Method: A Novel Method for Accurate Transponder RCS Calibration

Björn J. Döring*, Jens Reimann, Sebastian Raab, Matthias Jirousek, Daniel Rudolf, and Marco Schwerdt

Abstract—Transponders (also known as polarimetric active radar calibrators or PARCs) are commonly used for radiometric calibration of synthetic aperture radars (SARs). Currently three methods for the determination of a transponder's frequency-dependent radar cross section (RCS) are used in practice. These require either to measure disassembled transponder components, or a separate radiometric measurement standard (like a flat, metallic plate or a corner reflector), leading to additional uncertainty contributions for the calibration result. In this paper, a novel method is introduced which neither requires disassembly nor an additional radiometric reference. Instead, the measurement results can be directly traced back to a realization of the meter, lowering total measurement uncertainties. The method is similar in approach to the well known three-antenna method, but is based on the radar equation instead of Friis transmission formula. The suitability of the method is demonstrated by a measurement campaign for DLR's three new *Kalibri* C-band transponders, completed by an uncertainty analysis. The method is not universally applicable for all transponder calibrations because (a) three devices are necessary (instead of only one for the known methods), and (b) the transponders must provide certain additional features. Nevertheless, these features have become standard in modern SAR calibration transponder designs. The novel, potentially more accurate three-transponder method is thus a viable alternative for transponder RCS calibration, ultimately contributing to synthetic aperture radars with a reduced radiometric measurement uncertainty.

1. INTRODUCTION

Transponders, or polarimetric active radar calibrators (PARCs), are devices which are used as point targets for the radiometric calibration of space- or airborne synthetic aperture radar (SAR) instruments [2, 4, 9, 21]. Transponders consist of a receiving antenna, a very stable amplifier loop, and a transmit antenna [1, 6, 13]. The higher the total loop gain (antenna gains and electronic amplification) the brighter a transponder will appear in an acquired grayscale SAR image. If the transponder loop gain and its uncertainty is known prior to an overpass, then the transponder can be used as a measurement standard for the radiometric calibration of a SAR instrument.

Utilizing a transponder as a radiometric measurement standard requires the accurate radiometric calibration of the transponder itself. As a dominant contributor to the radiometric uncertainty budget for a SAR instrument, the quality of the transponder calibration has a direct impact on the overall radiometric measurement uncertainty of the SAR instrument. Currently, three methods are used in practice for the calibration of a transponder's frequency-dependent radar cross section (RCS), with varying advantages and disadvantages. These will be shortly reviewed in Section 2.

In the following Section 3, the novel three-transponder method (3TM) is introduced. Similarly to the popular three-antenna method [15], the new method allows to determine the unknown RCS of three transponders through three far-field measurements with two devices each. No additional radiometric

---

* Corresponding author: Björn J. Döring (bjoern.doering@dlr.de).
The authors are with the Microwaves and Radar Institute, DLR (German Aerospace Center), Germany.

reference (like a flat, metallic plate or a metallic corner reflector) is needed, eliminating a significant contribution to the radiometric uncertainty budget.

The applicability of the new method is demonstrated by calibrating DLR's three new C-band *Kalibri* transponders [13]. The measurement setup, the results, and an uncertainty analysis are given in Section 4.

The main advantages of the novel approach are that the transponders are measured in their final configuration (no parts are disassembled for the measurement), and that metrological traceability is established through length measurements, which in practice can be executed with low relative uncertainty. These two elements describe a transponder calibration approach which compares very favorably against the three approaches in use today, and in the end can lead to lower overall radiometric uncertainties in calibrated SAR instruments.

2. REVIEW OF EXISTING TRANSPONDER RCS CALIBRATION STRATEGIES

In this section several existing transponder RCS calibration approaches including their advantages and disadvantages are reviewed (also see [18]). This helps to stress the innovation of the novel approach in Section 3.

Measuring the loop gain. The radar cross section of a transponder can be determined by separately characterizing the gains of the components or component assemblies of a transponder which constitute the amplification loop. The necessary relationship between component gains and the transponder RCS ς_t was derived by Brunfeldt and Ulaby [1] and is based on the radar equation.

Using the symbols for the transponder components as introduced in Fig. 1(a) (right), the transponder RCS ς_t is given by [1]

$$\varsigma_t = \frac{\lambda^2}{4\pi} G_{tr} G_e G_{tt}. \tag{1}$$

In practical terms Eq. (1) means that the two antenna gains G_{tr} and G_{tt} can be conveniently measured in an antenna measurement test range and the electronic loop gain G_e can be determined by network analyzer measurements in a laboratory. This approach has been used to calibrate transponders for the TerraSAR-X mission calibration campaign [4, 21].

The disadvantages of the method are that component (e.g., antenna) mismatches cannot be characterized in the final configuration because the transponder components are measured in a disassembled state. Also, systematic offsets for absolute antenna gain measurements are often in the order of 0.1 dB, but can exceed 0.4 dB between any two measurement chambers as range cross calibration campaigns have shown [8]. This uncertainty has to be accounted for twice (both for receive and transmit paths) because the two required measurements are correlated. Therefore, the uncertainty in measuring the antenna gains alone results in total uncertainties which are large in comparison to the uncertainties expected for the two methods described in the following.

The substitution method. The second measurement approach is the most common measurement method for determining the RCS of any object: the substitution method. This approach requires a stable radar and a measurement standard (like a flat plate or a corner reflector) with a known radar cross section ς_{ref}. In a first step, the radar records the received power $P_r^{(\text{ref})}$ which results from measuring the reference target. In a second step, the reference is replaced by the unknown radar target, and under the assumption of a linear system, the RCS of the unknown target ς_{DUT} can be derived through proportionality from the second receive power P_r^{DUT}:

$$\varsigma_{\text{DUT}} = \frac{P_r^{(\text{DUT})}}{P_r^{(\text{ref})}} \varsigma_{\text{ref}}. \tag{2}$$

Different realizations of this scheme are possible. The most typical ones depend on (possibly compact) indoor or outdoor measurement ranges [14]. Alternatively, one can also use a SAR instrument to directly measure the transponder's equivalent radar cross section (ERCS) [3], an approach which is described in detail in [5].
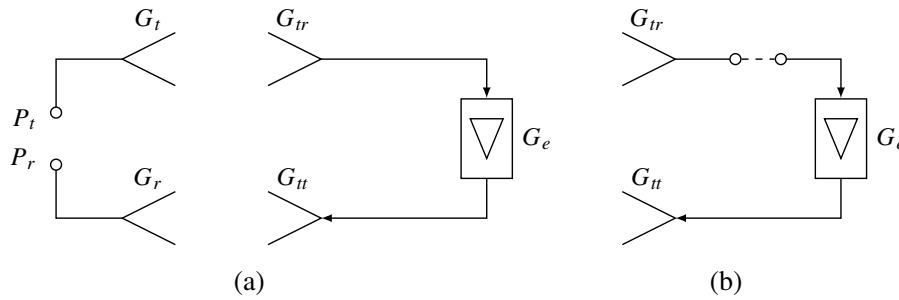
Figure 1. Different transponder configurations for transponder RCS measurements. (a) Schematic diagrams of a radar (left) and a transponder (right). (b) Block diagram of a transponder which can also be operated as a radar, i.e., the amplifier loop can be opened.

The advantages of the approach are the end-to-end nature of the measurement setup. Ideally, the transponder does not need to be disassembled. A disadvantage is the need for an additional radiometric reference, whose radiometric uncertainty defines a lower bound on the achievable transponder calibration uncertainty. Also, outdoor ranges typically suffer from not perfectly controllable conditions leading for instance to multipath effects.

Shielded indoor ranges, on the other hand, pose another challenge: A transponder is basically a high gain open amplifier loop with a high receiver sensitivity. Stray (noise) signals which are not sufficiently suppressed by the chamber's absorbers are picked up and can lead to resonance and saturation of the transponder electronics. A practical workaround implemented by the authors in a different campaign was to introduce an additional attenuator in the amplifier loop, which can suppress resonance but also requires modifications of the amplification loop after transponder calibration.

The transponder as a radar instrument. The third known method for deriving the RCS of a transponder combines ideas from the first two approaches and was introduced for the characterization of the European Remote Sensing Satellite 1 (ERS-1) transponder by Jackson and Woode [12]. If the transponder can be operated as a radar, i.e., if the transponder loop can be opened (see Fig. 1(b)), then the measurement of the ratio of the received over the transmitted power, the knowledge of the RCS of an external reference, and the knowledge of the distance between the reference and the transponder is sufficient to derive the transponder RCS. Assuming a conducting, circular, flat plate with a surface area A_p as the radiometric reference, then the transponder RCS can be derived [12]:

$$\varsigma_t = 4\pi \frac{P_{tr} \lambda^2 R^4}{P_{tt} A_p^2}. \tag{3}$$

The advantage of the approach is that the transponder can be measured in its final configuration (provided it was designed for opening the amplification loop), and no additional measurement device like an expensive network analyzer is needed. Some disadvantages arise in practical implementations: The limited transmit/receive decoupling of the transponder antennas typically requires very short pulses or long distances, so that transmission and reception are separated in the time domain. If the reference plate is installed on a remote site (e.g., the roof of a house), then sufficient time-gating in post-processing for background removal is not an option because of the limited bandwidth of most transponders (leading to large time gates). Further problems typically found in other outdoor measurement setups like multipath are similar with respect to the substitution method described above. Also, any pulsed method does not yield the transponder RCS at a single frequency, but as a weighted average of the RCS over the pulse bandwidth (see discussion on RCS vs. ERCS in [3, 7]), which results in a mismatch between what shall be measured (RCS over frequency) and what is measured (single weighted RCS average).

Radar Equation Another approach, which is typically not used in practice due to inherently large measurement uncertainties, is based on the radar equation:

$$P_r = P_t \frac{G_r G_t \lambda^2 \varsigma_t}{(4\pi)^3 R^4}. \tag{4}$$

The equation describes a radar instrument's received power P_r by an antenna with gain G_r as a function of a target's (i.e., transponder's) scattering cross section ς_t at a far-field distance R, and the radar's power P_t transmitted by an antenna with gain G_t at a wavelength λ. The transponder RCS can be derived if all other quantities are known. While this approach is conceptually simple, it requires an absolute knowledge of all other quantities (including absolute antenna gains), resulting in comparably large measurement uncertainties, so that to the best of our knowledge this approach has not been used in practice for transponder RCS calibrations.

3. THE THREE-TRANSPONDER METHOD PRINCIPLE

In Section 3.2, the measurement principle behind the novel three-transponder method (3TM) will be introduced, which can be used for the RCS calibration of three or more transponders. No additional radiometric reference target (e.g., a trihedral reflector with an accurately known RCS) is required for the measurement, but certain restrictions on the transponder design are imposed, which are discussed beforehand in the following Section 3.1.

The three-transponder method is an advancement of the well known three-antenna method [15], which is used to determine the gains of three unknown antennas. The three-antenna method is to-date the most accurate method for determining antenna gains, down to a reported uncertainty of $\pm 0.05\,\mathrm{dB}$ [15].[†] The proposed three-transponder method might result in similarly accurate transponder RCS measurements in the future.

3.1. Prerequisites on Transponder Design

The three-transponder method as described below is only applicable for a certain transponder type. Specifically, two out of three transponders must not only be operable as radar targets *but also* as a radar, i.e., the transponder must be able to emit and record radar signals within the transponder bandwidth. One possible implementation is shown in Fig. 2 where the transponder's receiving (RX) and transmitting (TX) paths are connected through a digital unit. The three C-band transponders developed and built by DLR from 2009 to 2014 fulfill this requirement [6].

The (by design exactly known) digital amplification (DA) is permitted to be different from 1. In Fig. 2(a), the digital amplification is counted toward the TX path. Here, coupling the digital signals out or in (for transmission or recording) is implemented at the same location in the amplification loop, so that the digital amplification does not need to be treated separately from the analog amplification.
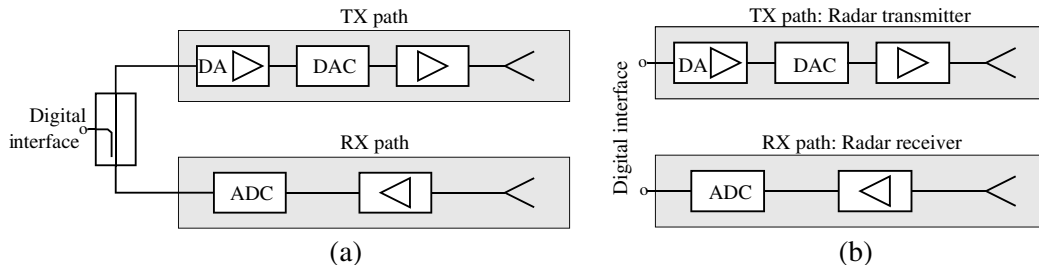

Figure 2. Principal required transponder design: An operation as a radar target *and* as a radar instrument are both possible. The digital signal is coupled out and in at the same location; a possible digital amplification (DA) is part of the TX path. (a) Device operated as a transponder. (b) Device operated as a radar.

[†] Kummer and Gillespie [15] do not state precisely what they understands by the term *uncertainty*. Considering the publication year 1978, their definition does most likely not coincide with the term *standard uncertainty* [11] used otherwise in this paper.

3.2. System of Linear Equations

The three-antenna method is based on the threefold application of Friis transmission formula to make three independent gain measurements with three-antennas [15]. In contrast, the three-transponder method is based on the threefold application of the radar equation to make three independent RCS measurements of three transponders. Each RCS measurement is performed by one of the three transponders (operated as a radar), whereupon the radar target under test is one of the other two transponders (operated as a transponder), see Fig. 3.
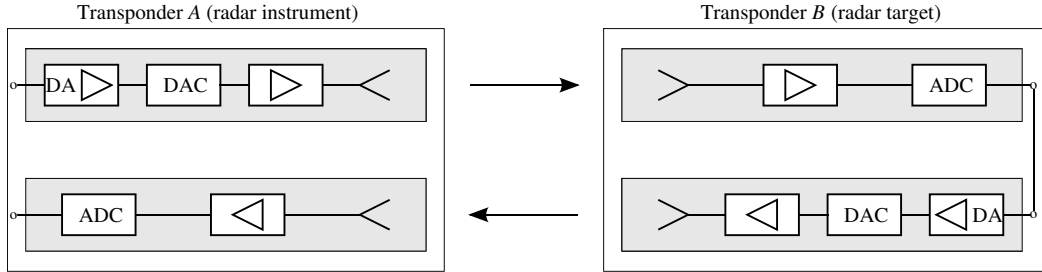
Figure 3. Three-transponder method measurement setup.

The first essential equation for the method is the radar Eq. (4). The second required equation describes a transponder's radar cross section ς_t by its loop gain G_l (cf. Eq. (1)). It is given as [1]

$$\varsigma_t = \frac{\lambda^2}{4\pi} G_l, \tag{5}$$

where the total loop gain is usually decomposed as $G_l = G_t G_e G_r$, i.e., the multiplication of the transponder's transmitting and receiving antenna gains, and the electronic amplification G_e. In the nomenclature of Fig. 2(a), this can be expressed as

$$\varsigma_t = \frac{\lambda^2}{4\pi} G_{tx} G_{rx}, \tag{6}$$

where G_{rx} and G_{tx} are the gains of the RX and TX paths (including the ADC, DAC, and digital amplification). The gains of the TX and RX paths are a combination of electronic amplifications and antenna gains.

The two Eqs. (4) and (5) can be combined into one. Assuming that transponder A is operated as a radar and transponder B as a radar target (abbreviated as combination AB), it follows that

$$\left.\frac{P_r}{P_t}\right|_A = \frac{\lambda^2}{(4\pi)^3 R^4} \cdot \frac{4\pi}{\lambda^2} \cdot \varsigma_A \cdot \varsigma_B. \tag{7}$$

By exchanging the transponders, two more equations for the combinations AC and BC can be derived.

The resulting three equations can be converted to a linear set of equations by logarithmic transformation. This is possible because all terms are larger than zero. For convenience the same symbols are used for the transponder RCS, but it is understood that they refer to values expressed in decibel, i.e., after the transformation $10 \log(\cdot)$. Hence, Eq. (7) can be expressed as [‡]

$$\varsigma_X + \varsigma_Y = P_{XY} + C, \tag{8}$$

with P_{XY} being the ratio $10 \log(P_r/P_t)$ measured by device X and using device Y as the radar target. All known terms are summarized in

$$C = 20 \log(4\pi R^2). \tag{9}$$

The linear set of equations can now be expressed in matrix form

$$\begin{pmatrix} 1 & 1 & 0 \\ 1 & 0 & 1 \\ 0 & 1 & 1 \end{pmatrix} \begin{pmatrix} \varsigma_A \\ \varsigma_B \\ \varsigma_C \end{pmatrix} = \begin{pmatrix} P_{AB} \\ P_{AC} \\ P_{BC} \end{pmatrix} + C. \tag{10}$$

[‡] For brevity, a normalization cross section $\varsigma_0 = 1\,\mathrm{m}^2$, which is required to convert values with dimension $[\mathrm{m}^2]$ to dimensionless values before taking the logarithm, was omitted. In logarithmic form, the RCS ς is then given in [dBsm].

Inverting the matrix yields the three unknown transponder cross sections

$$
\begin{pmatrix} \varsigma_A \\ \varsigma_B \\ \varsigma_C \end{pmatrix} = \frac{1}{2} \begin{pmatrix} 1 & 1 & -1 \\ 1 & -1 & 1 \\ -1 & 1 & 1 \end{pmatrix} \begin{pmatrix} P_{AB} + C \\ P_{AC} + C \\ P_{BC} + C \end{pmatrix}.
\tag{11}
$$

In summary, the three unknown transponder radar cross sections are determined by completing three measurements with different pairs of transponders, where one transponder is operated as a radar during each measurement. Each measurement is performed at a single frequency (using a sine tone). The measurements can be repeated in a stepped frequency fashion in order to determine the frequency dependent transponder RCS within the transponder bandwidth.

It is interesting to note that only a length measurement (R in Eq. (9)) needs to be traced back to a national standard in order to establish calibration traceability.

It is not important which transponder is operated as a target and which one as a radar within each of the three measurement combinations. In a set of measurements AB, AC, BC only the two transponders A and B need to be operated as radars, and only transponders B and C need to be operated as transponders. Therefore, only transponder B needs to be operated as a radar *and* a transponder during the measurement campaign, relaxing the hardware requirements for devices A and C.

If the RCS of more than three-transponders shall be determined, more transponder measurement combinations are possible according to

$$
\binom{n}{2} = \frac{n!}{2(n-2)!}
\tag{12}
$$

where n is the number of transponders. For a set of four transponders, a total of 6 transponder combinations become possible, resulting in six distinct measurements. The resulting matrix similar to Eq. (10) then has a shape of 6×4; the linear system of equations is overdetermined. This property might be exploited in a probabilistic sense in order to derive the most probable set of radar cross sections when measurement uncertainty is considered. It can be noted though that for each additional transponder, one additional measurement is sufficient. This is because the RCS's of the first three transponders were determined with Eq. (11), and the RCS of each additional transponder can then directly be determined through Eq. (7). Every additional device only needs to be operable as a transponder, i.e., not as a radar.

4. DEMONSTRATION MEASUREMENT CAMPAIGN WITH *KALIBRI* C-BAND TRANSPONDERS

The first demonstration of the novel method described above was set up to calibrate the frequency-dependent RCS of DLR's new three C-band *Kalibri* transponders [6, 13], which have subsequently been used for the calibration of Sentinel-1 [22]. The *Kalibri* transponders down-convert and digitize the incoming signal for an adaptable delay and real-time signal filtering before the regenerated signal is up-converted, amplified, and retransmitted again. The transponder design with a digitizing unit in the signal path makes them an ideal fit for the demonstration of the three-transponder method.

The transponder RCS measurement campaign was completed within two weeks in December 2013. An appropriate outdoor measurement range for the demonstration campaign did not exist at DLR so that an ad hoc measurement range needed to be set up. During measurements, two transponders were placed in the far-field of each other on the roofs of adjacent buildings, which reduced multipath contributions considerably. Although the ad hoc range worked very well for the first demonstration of the three-transponder method, future and more accurate measurements would require a dedicated antenna measurement range with improved multipath suppression.

4.1. Measurement Setup

The three-transponder method procedure requires three transponders to be measured against each other with at least three measurements. As above, the three pairs of measurements are denoted with AB, AC, and BC, where the mapping from transponder name to letter is shown in Table 1 for completeness.

Table 1. Mapping between transponder device names and symbols as used in Eq. (11) for the three-transponder method (3TM), and additional attenuators used during the campaign.

Device name	3TM letter	Attenuator [dB]
Kalibri 1	C	21.87
Kalibri 2	A	21.99
Kalibri 3	B	22.11

The goal of the three-transponder method is to derive the frequency dependent RCS of all three transponders. The RCS is only meaningfully defined for the far field. With a maximum antenna dimension D, the far-field region is commonly defined for distances R fulfilling

$$R > \frac{2D^2}{\lambda},\tag{13}$$

where λ is the wavelength [23]. Here, transponders with two antennas are used, where each antenna aperture has a diameter of about 20 cm, and the antenna feeds are separated by about 40 cm. Therefore, with a D of 60 cm and a wavelength at C-band of 5.6 cm, the far field approximately begins 13 m away from the transponders.

An ad hoc far-field range was installed at the DLR site in Oberpfaffenhofen which fulfills the far-field requirement. The transponders were installed about 45 m apart on the roofs of two adjacent buildings, see Fig. 4. The elevated position attenuates possible multipath contributions from the ground due to the longer path lengths. The transponder on the KN building was installed on a *Kalibri* elevation-over-azimuth, remote-controlled positioner unit, facilitating easy alignment of the transponder along the line-of-sight. The second transponder on the HR building was mounted on a custom-built motorized slide, which itself was accurately aligned with the line-of-sight between the two transponders. The slide axis allows to repeat measurements at varying transponder-to-transponder distances to detect a possible standing wave due to multipath effects. The maximum traversing range of the slide is 95 cm.
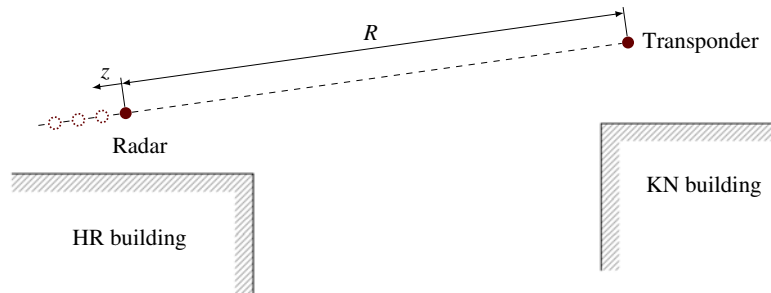
Figure 4. Side view of the measurement setup with two transponders installed on the roofs of two adjacent buildings. The solid circles denote the transponder antenna phase centers. Dotted circles indicate additional slide positions for the transponder on the HR building.

All RCS measurements reported here were performed in main beam direction of the transponders. All antennas were rotated by 45° with respect to the vertical (the nominal configuration for SAR calibration transponders). The transmitting antenna of one transponder was always co-polar aligned with the receiving antenna of the other transponder.

An accurate alignment of the transponders' main beam directions was achieved with a laser and mirrors, which were mounted on the transponder structures between the antennas. The approach is described in detail in [17]. The distance $R = 46.0$ m at a slide position of $z = 0$ cm was measured with a tachymeter, whose recent calibration can be traced back to national standards.

All 3TM measurements were performed in an automated fashion. Generally, the transponder on the HR building was operated as the radar device (transmitting a programmed signal, and subsequently

recording it again), and the transponder on the KN building as the transponder device (delayed retransmission of the received signal). In order to reduce multipath effects, the timing of the transmit signal and the delay of the KN transponder was finely tuned to exclude most multipath effects. The transmit signal consisted of 1001 short (0.25 µs long) continuous wave pulses interrupted by 1.35 µs pulse pauses, covering the complete 100 MHz wide transponder bandwidth. A pulse length of below 0.3 µs at a two-way distance between the buildings of about 90 m ensured that strong reflections from the facade of the KN building are filtered out in time domain. In order to decouple transmission and reception for the HR transponder, the programmable delay for the KN transponder was set to 0.9 µs.

The amplitude of the transmit signal was programmed to an analog-to-digital converter code of 368 (out of 511). This ensured that the transponders were measured at the same operating point which is expected during later satellite overpasses.

The loop gain of the transponders needed to be reduced for the measurement campaign because the short distance between the transponders (due to the implemented ad hoc measurement setup) and the large transponder output power would drive the receiving chain into saturation. Each measured transponder was therefore fitted with an additional fixed attenuator, which was inserted into the transponder loop just before the transmit antenna so that the internal transponder gain correction was not affected. The required attenuation was about 22 dB; accurately measured attenuations (measured with three network analyzers) for each of the three attenuators are listed in Table 1.

Although the main multipath contribution resulting from the reflection of the signal by the KN building facade is removed in time domain, a second multipath contribution could not be avoided. The second major reflection occurs due to the metallic building protrusion in front of the HR transponder. As will be shown later, reflections from this protrusion result in an undulation of the receive signal for varying slide positions. As a remedy, some later measurements were performed with flat outdoor wideband foam absorbers covering the protrusion. The two sets of measurements (without and with absorbers) will be compared with each other in the following Section 4.2 because a comparison of the final measurement results also serves as a check of plausibility.

For each of the three measurement pairs AB, AC, BC[§], measurement data was recorded for 96 z (slide) positions at 1 cm increments. At each position, a single signal with 1001 pulses as described above was transmitted and recorded by the HR device. After recording, a threshold analysis of the received signal in time domain allowed to extract the pulse root-mean-square (RMS) amplitudes of all 1001 pulses, which were then stored along with the z position in a database for later analysis.

All measurements were completed at fair weather, so that radiometric effects due to the atmosphere, humidity, or ice covering the antenna apertures can be excluded. Furthermore, an internal gain correction was performed for each transponder prior to every sweep, ensuring a constant transponder RCS (within the short-term transponder gain stability) throughout all measurements.

4.2. Measurement Data Analysis

Strictly speaking, the three-transponder method requires nothing more than measuring the receive-to-transmit power ratios P_{XY} for the three transponder combinations AB, AC, and BC at broadside alignment and at a known distance R, and substituting the measured values into the system of linear Eqs. (11). The measurements and computations might be repeated for all frequencies of interest.

In practice, it is highly desirable to derive a standard measurement uncertainty along with the derived transponder RCS's. To estimate the uncertainty and to possibly lower it through exploitation of additional information (repetitions), it is advantageous to perform more than the strictly required number of measurements. Here, one of the main uncertainty contributions was assumed to be multipath due to a non-optimal outdoor measurement range. Therefore, measurements were repeated at varying slide positions.

In the following, two measurement triplets shall be analyzed. For the first triplet, no foam absorbers were used to cover the protrusion at the HR site. In contrast, flat foam absorbers were used to cover the protrusion for the second triplet.

The original RMS receive amplitudes for sweeps AB, AC, and BC are shown in Fig. 5 for both measurement triplets. A standing-wave pattern is clearly apparent. The RCS of the three transponders

---

[§] Again, the first letter denotes the radar device, and the second letter the transponder device.

is independent of z axis position, which should ideally be reflected by horizontal lines in Fig. 5. Instead, the receive power varies by more than 0.5 dB for sweep AB in Fig. 5(a) for z ranging from 45 cm to 70 cm, for instance.[‖]
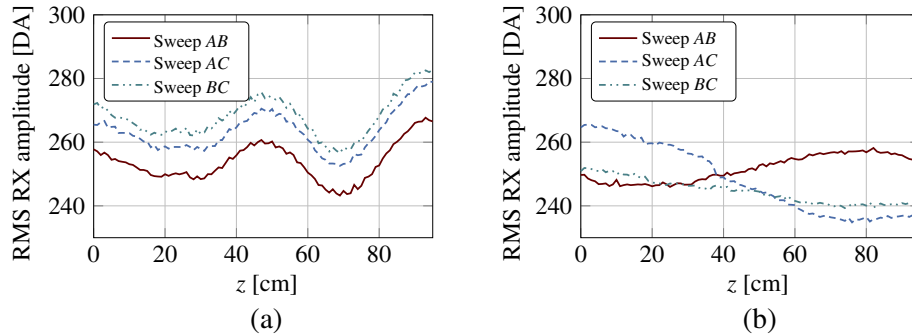
Figure 5. Original received RMS amplitude (in digital amplitude (DA) or ADC codes) in dependence of slide position z for two different sweep triplets at the center frequency. (a) Without absorbers. (b) With absorbers.

It can be observed that only for sweep BC in Fig. 5(b) (measurement with absorbers) the amplitude of the undulation appears greatly reduced. For the other two sweeps in Fig. 5(b), the absorbers mostly affect the period (and therefore the multipath geometry) and not so much the amplitude. The explanation most likely lies in the angular dependent reflectivity coefficient of the absorbers. The foam absorbers were laid out flat on the protrusion, resulting in flat angles of the multipath ray. At these angles, the effectiveness of the foam absorbers is much reduced in comparison to normal incidence angle — a fact which was unfortunately only considered after completion of the measurement campaign. Nevertheless, the absorbers have helped in producing a more regular undulation pattern, simplifying analysis.

Before the data at different slide positions can be exploited in subsequent steps, the varying free-space path loss for different slide positions z (proportional to $(R + z)^4$ according to the radar Eq. (4)) needs to be compensated. The transponder-to-transponder distance R was measured at $z = 0$ cm, so that all data is normalized here to R at $z = 0$ cm. The resulting distance-compensated data is shown in Fig. 6.
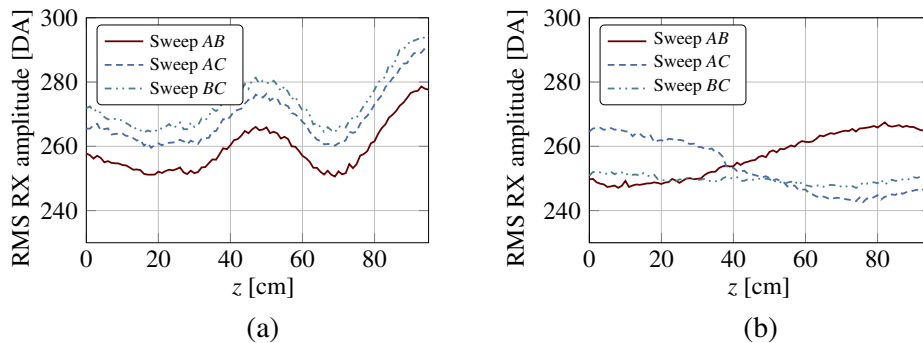
Figure 6. Received RMS amplitudes from Fig. 5 normalized for a far-field distance R at $z = 0$ cm for the two different sweep triplets. The slight downward drift of the curves in Fig. 5 for increasing z appears removed. (a) Without absorbers. (b) With absorbers.

Knowing the transmit amplitudes (from the configured transmit signal amplitude), a set of 96 power ratios P_{AB}, P_{AC} and P_{BC} can be derived, covering all z positions. A highly over-determined linear system of Eq. (11) results, which most likely does not have a solution (due to noise of the

---

[‖] The value in decibel is equivalent to an amplitude difference of 15 DA at a reference amplitude of 253 DA.

measured samples). One might be tempted to solve this overdetermined system of equations with a multivariate regression analysis and the method of least squares. This approach readily results in one RCS per transponder, but it violates several assumptions which are required for this kind of regression analysis [10, 19], suggesting wrong conclusions. First, the error terms (difference between estimated and measured values) are not normally distributed, and second, the error terms do not result from independent observations with common variance. The violations are a direct consequence of the strong dependence of measured data on z (because of multipath effects), where ideally samples scattered normally around a horizontal line would be expected.

According to the ANSI/IEEE Standard 149-1979 (IEEE Standard Test Procedures for Antennas), the recommended approach for removing multipath effects (undulations) from measured data for varying slide positions is averaging. For this, several periods of the standing wave pattern should be recorded to get accurate results. Unfortunately, the geometry (flat angle of arrival for the multipath ray) produced a pattern with not even two full periods within the slide range, see Fig. 6(a). Therefore, another approach was sought.

In order to estimate the transponder RCS's (and their standard uncertainties) under the standing wave assumption, the standing wave is modeled and approximately removed from the data. To this end, a single dominant, coherent reflection is assumed. The reflection signal interferes with the much stronger direct path signal at the receiver, resulting in a standing wave in z direction. If the reflected signal and the direct path signal are assumed to have a constant amplitude independent of slide position z, then the measured RMS receive amplitude A_{XY} (where again X denotes the device operated as a radar, and Y denotes the device operated as a transponder) can be modeled as a constant RMS amplitude $\hat{A}_{XY}$ resulting from the direct path signal, and a sinusoidal undulation with amplitude a, period $1/f$, and phase offset θ according to

$$A_{XY} = \hat{A}_{XY} + a \sin(2\pi f z + \theta). \tag{14}$$

This model can be applied for any slide sweep within one triplet, defining $\hat{A}_{AB}$, $\hat{A}_{AC}$, and $\hat{A}_{BC}$.

Once the three multipath-corrected signal RMS amplitudes $\hat{A}_{AB}$, $\hat{A}_{AC}$, and $\hat{A}_{BC}$ have been estimated, the receive to transmit power ratios P_{AB}, P_{AC}, and P_{BC} can be derived. Together with Eq. (11), one yields the three transponder RCS's.

The model of Eq. (14) is fitted to the measured data through Bayesian data analysis and the Monte Carlo Markov Chain (MCMC) approach. The immediate advantage of this approach is that all estimated model parameters like $\hat{A}_{XY}$ are treated as probability densities, which characterize the uncertainty with which the parameters are estimated. Highest probability density intervals for all estimated and subsequently derived parameters (transponder RCS's) can easily be stated.

One Bayesian hierarchical model is created per sweep triplet per frequency. For each transponder combination and frequency, the model parameters $\hat{A}$, a, and θ are assumed to be different, whereas f is assumed to be identical for all measurements within a triplet (f is a hyperparameter for the model). This assumption is not only physically sound (the geometry between the sweeps is mostly identical), it also seems to be a good assumption given the observed data.

The Bayesian model requires priors (probability density functions) for all parameters before parameter estimation. These are summarized in Table 2. The parameters are then estimated numerically with the Monte Carlo Markov Chain approach. For each model evaluation, 100 000 samples are drawn. The first 3000 samples are discarded, and only every 300th is recorded for an improved sample-to-sample independence.

In order to verify that the model can reasonably well represent the data, the last 100 sampled fitted sine curves are superposed on the measured sweep data in Fig. 7. For sweeps with absorbers, the sinusoidal fits seem to closely follow the measured data. Sweeps without absorbers, on the other hand, are less well represented by the model. Instead of fitting a single sine curve, a more complex model with two or more sinusoidal functions would be required to better separate the direct and multipath components. Yet, the limited data available does not justify the derivation of model parameters of a more complex model because for that a larger traversing range (or a different measurement geometry) would be required. In the end, differences between the model and measured data have to be accounted for in an additional uncertainty analysis because the uncertainty components cannot be estimated from the data directly.

Table 2. Priors for the hierarchical Bayesian model used to fit a sine curve to each of the measured RMS amplitudes from Fig. 6. All priors are identically chosen for the two sweep triplets except for f, which is constrained in order to achieve a faster model convergence. Note on notation: $U(a, b)$ denotes a uniform distribution with lower and upper bounds a and b; $N(\mu, \sigma^2)$ denotes a normal distribution with mean μ and standard deviation σ.

Variable	Prior	Count
$\hat{A}$	$N(\mu, \sigma^2)$	3
μ	$U(100, 400)$	3
σ	$U(0, 40)$	3
a	$U(0, 25)$	3
θ	$U(0, 2\pi)$	3
f_1	$U(0.2, 1)$	1
f_2	$U(1, 5)$	1

Now having estimated the probability density functions for $\hat{A}_{XY}$ for all frequencies, the frequency dependent transponder RCS's can be computed with Eq. (11). The computation step can be done directly within the numerical Bayesian model so that the output quantities are also given as probability density functions. A summary of the computations is shown in Fig. 8, where the best estimate along with the 95% highest probability interval is shown. Superimposed are some earlier (normalized) network analyzer (NWA) transmission measurements, which show the principal frequency response of each transponder. The network analyzer measurements cannot include the frequency response of the antennas, and this explains some of the differences between the NWA and the three-transponder method measurements. In principle, a remarkable resemblance between the NWA and three-transponder method curves can be observed, stressing that the novel three-transponder method principle works.

Table 3 summarizes the RCS's of all three transponders at the center frequency. Again, the non-overlapping 95% highest probability intervals for the two sweep triplets indicate that the model (14) is insufficient in explaining the data. A more detailed uncertainty analysis follows in the next section, addressing this issue.

Table 3. Intermediate results: Best transponder RCS estimates at the center frequency 5.405 GHz, the results of the Bayesian analysis applied to the two sweep triplets. Values in brackets denote the 95% highest probability density interval resulting *solely* from Bayesian model fitting. Non-overlapping intervals especially for device C indicate model errors.

Transponder	Without absorbers [dBm^2]		With absorbers [dBm^2]	
Device A (Kalibri 2)	66.15	$[66.09; 66.21]$	66.28	$[66.20; 66.37]$
Device B (Kalibri 3)	66.30	$[66.24; 66.35]$	66.10	$[66.01; 66.19]$
Device C (Kalibri 1)	66.62	$[66.56; 66.68]$	66.04	$[65.94; 66.14]$

4.3. Uncertainty Analysis and Results

The uncertainty analysis for the measured transponder RCS's is performed in accordance with the Guide to the Expression of Uncertainty in Measurement (GUM [11]). In short, the GUM approach depends on a measurement model relating the measurement quantity (transponder RCS ς in dBm^2) to the input quantities, assigning uncertainties (probability distributions) to the input quantities, and deriving the combined uncertainty for the output quantity through computations and the measurement model.
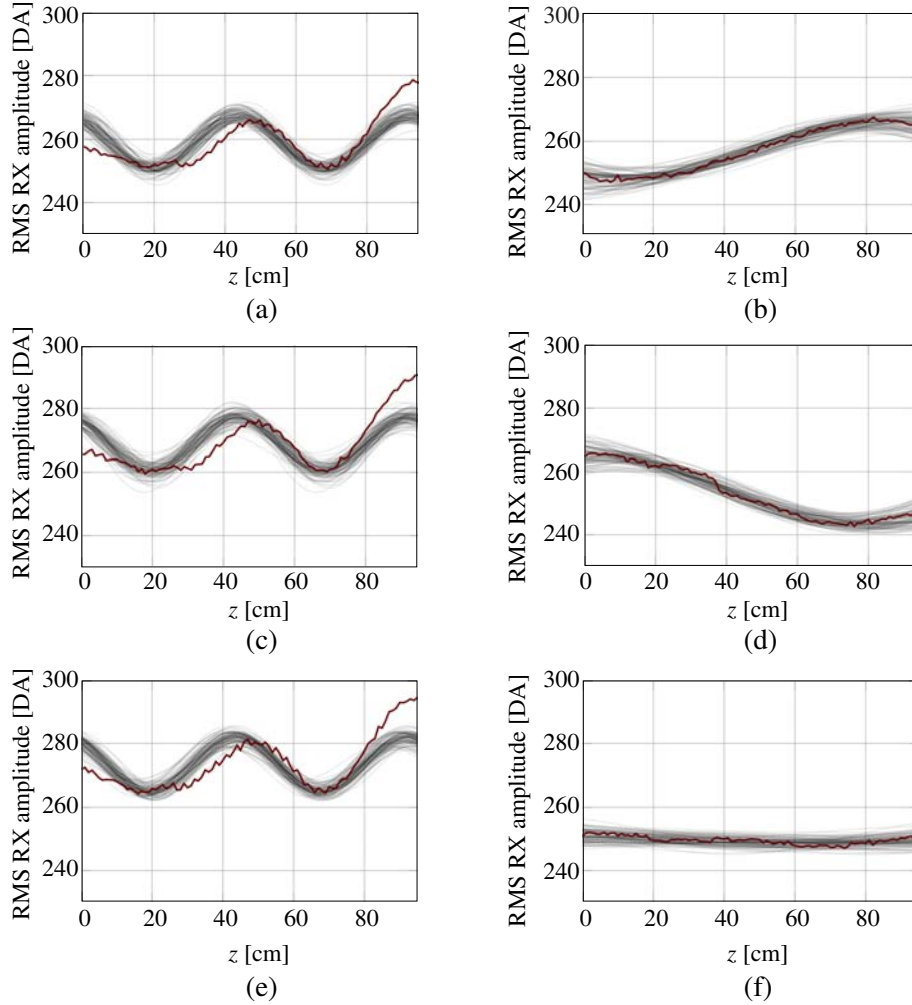
Figure 7. Received RMS amplitudes from Fig. 6 (thick line, at center frequency) and 100 random sine fits per curve. It becomes apparent that the model from Eq. (14) fits the recorded data better when absorbers are used. (a) Sweep AB, without absorbers. (b) Sweep AB, with absorbers. (c) Sweep AC, without absorbers. (d) Sweep AC, with absorbers. (e) Sweep BC, without absorbers. (f) Sweep BC, with absorbers.

From Eqs. (9) and (11), the measurement model is given as (for instance for device A):

$$\varsigma_A = \frac{1}{2}(P_{AB} + P_{AC} - P_{BC} + C) + D_A, \tag{15}$$

$$C = 20\log(4\pi R^2). \tag{16}$$

D_A refers to the attenuation of the additional attenuator in decibel (see Table 1), which was part of the measurement setup but is removed again afterward.

In the following sections, the individual uncertainties for the input quantities P_{XY}, C, and D_X are derived and finally combined to yield the overall uncertainty budget.

4.3.1. Uncertainties in Estimations of P_{XY}

P_{XY} is the ratio of the received power to the transmitted power in decibel, when device X is used as a radar and device Y is operated as a transponder. This ratio varies if the transponders are not perfectly aligned with each other, the transponder loop gain drifts during a measurement, or the antenna
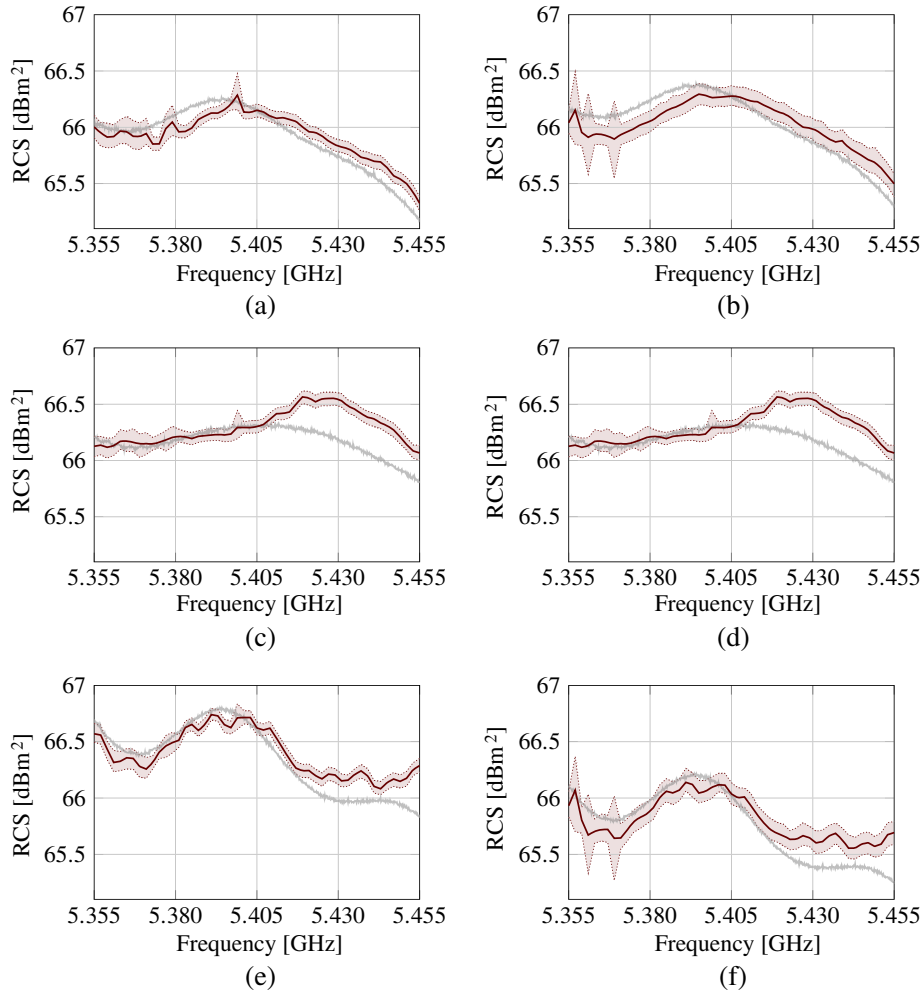
Figure 8. Estimated transponder RCS's in dependence of frequency resulting from Bayesian analysis and Eq. (11). The filled area between the dotted lines indicate the bounds for the 95% highest-probability density intervals (considering uncertainties in estimation of P_{XY} only). The gray, slightly noisy lines show network analyzer transmission measurements (necessarily excluding antennas) for comparison, normalized to estimated RCS at the center frequency. The network analyzer measurements follow the three-transponder method measurements encouragingly well. (a) Transponder A (Kalibri 2), no absorbers used. (b) Transponder A (Kalibri 2), measured with absorbers. (c) Transponder B (Kalibri 3), no absorbers used. (d) Transponder B (Kalibri 3), measured with absorbers. (e) Transponder C (Kalibri 1), no absorbers used. (f) Transponder C (Kalibri 1), measured with absorbers.

polarizations do not lie within the same plane. The uncertainties resulting from these contributions are given in the next paragraphs. The uncertainty in estimating P_{XY} from the data has been analyzed before, as summarized in Table 3.

Alignment errors. Ideally, the two transponders should be aligned in main-beam direction with respect to each other. Deviations from this main beam direction are a result of mechanical alignment errors during the alignment process (using a laser and mirrors), and of the fact that the main beam direction is, strictly speaking, frequency dependent.

The alignment uncertainty of each transponder is assessed to be 1°, which translates to a radiometric uncertainty of 0.03 dB due to the shape of the antenna pattern (known through previous transponder pattern measurements [16]).

Gain drift errors. Each measurement sweep across all slide values took about 1 h to complete. During this time, the transponder gain varies slightly despite the thermal control. Previous repeated measurements have shown that the transponder gain is stable within a standard uncertainty of 0.02 dB during 1 h intervals [5].

The uncertainty due to drift is remarkably low, but it could be reduced further in future measurements by interleaving internal gain corrections with the three-transponder method sweep measurements (and therefore reducing the time interval between subsequent internal gain corrections). The total measurement time would increase though.

Antenna misrotation. All antennas were operated at a nominal rotation of $\pm 45°$ with respect to the vertical direction (adjusted with a level). The transmitting antenna of one transponder and the respective receiving antenna of the other were always co-polar aligned with respect to each other.

A rotation which deviates from the nominal rotation results in a reduced received signal amplitude due to polarization mismatch. The sensitivity of P_{XY} on the angular deviation φ of an antenna, e.g., from device X, from perfect co-polar alignment can be derived from Eq. (7), which becomes

$$P_{XY}(\varphi) = 10 \log \left(\frac{\varsigma_Y}{16\pi^2 R^4} \right) + 10 \log(\hat{\varsigma}_X \cos^2 \varphi) \qquad (17)$$

after logarithmic transformation. Here, $\hat{\varsigma}_X$ denotes the RCS of device X without polarization loss.

Usually, one would determine the sensitivity coefficient of P_{XY} on φ by taking the partial derivative of P_{XY} with respect to φ at $\varphi = 0°$, under the assumption that P_{XY} is approximately linear around the point of evaluation ($\varphi = 0$) [11]. The linearity assumption is not fulfilled here; the sensitivity coefficient would become zero. Instead of computing the partial derivative, the resulting uncertainty can be approximated by evaluating Eq. (17) at the two close values $\varphi = 0$ (ideal alignment) and $\varphi = 1°$ (estimated rotation uncertainty). The difference, which reduces to $20 \log(\cos 1°) = 0.001$ dB, yields the uncertainty in P_{XY} due to antenna misrotation.

Additional propagation path attenuation. Water drops or thin layers of ice on the transponder aperture covers can result in a modified value for P_{XY}. For the completed measurements, it was ensured that no humidity or ice was covering the apertures. Furthermore, no measurements were taken in heavy precipitation conditions so that no additional propagation path losses need to be considered in the following.

Combined standard uncertainty for P_{XY}. Table 4 summarizes all uncertainties described above which contribute to uncertainties in P_{XY}. Note that many contributions appear twice, i.e., once per transponder. The contributions are assumed to be mutually uncorrelated, so that the combined relative standard uncertainty of 0.07 dB results from the rule of root-sum-square [11].

Table 4. Mutually uncorrelated standard uncertainties u contributing to a combined standard uncertainty for estimates of P_{XY} (according to the GUM [11]).

Contribution	Value	u [dB]
$\hat{P}_{XY}$ estimation (Bayesian analysis)		0.05
Alignment error X	1°	0.03
Alignment error Y	1°	0.03
Gain drift X		0.02
Gain drift Y		0.02
Antenna misrotation X (polarization)	1°	0.001
Antenna misrotation Y (polarization)	1°	0.001
Additional propagation path attenuation		0
Resulting combined standard uncertainty for P_{XY}		0.07

4.3.2. Top-Level Uncertainties

The combined standard uncertainty u_c for the transponder RCS's follows from deriving sensitivity coefficients c_i for all N input quantities x_i, estimating the standard uncertainties $u(x_i)$ of the input quantities x_i, and then taking the positive square root of the combined variance, given as [11]

$$u_c^2(\varsigma) = \sum_{i=1}^{N} \left(\frac{\partial \varsigma}{\partial x_i} \right)^2 u^2(x_i) = \sum_{i=1}^{N} [c_i u(x_i)]^2. \tag{18}$$

This is under the assumption that all uncertainties $u(x_i)$ are mutually uncorrelated.

The following sections address the separate input quantities x_i from Eq. (15), and the derivation of the respective sensitivity coefficients c_i. Finally, the combined uncertainty is computed.

Estimates of P_{XY}.   The absolute value of the sensitivity coefficients c_P for the input quantities P_{AB}, P_{AC}, and P_{BC} are identical and given by

$$|c_P| = \left| \frac{\partial \varsigma}{\partial P_{AB}} \right| = \left| \frac{\partial \varsigma}{\partial P_{AC}} \right| = \left| \frac{\partial \varsigma}{\partial P_{BC}} \right| = \frac{1}{2}. \tag{19}$$

The value of $u(P_{XY})$ was given in the last row of Table 4.

Multipath model error.   The previous uncertainty for P_{XY} does not contain a term which addresses inconsistencies observed before. Measurements with and without absorbers resulted in significantly different values for P_{XY} (see Fig. 7), which consequently resulted in different derived RCS's (see Fig. 8). The inconsistency was attributed to the multipath model in Eq. (14), which apparently is too simple to explain the observed undulations in P_{XY}.

In order to quantify the model error, the worst-case difference between estimated $\hat{P}_{XY}$ with and without absorbers at the center frequency shall be taken. This certainly discussible approach results in an estimated model uncertainty of 0.75 dB (see Figs. 7(e) and 7(f)).[¶]

The value dominates the overall uncertainty budget, and it is therefore especially unfortunate that a more objective approach cannot be devised for estimating this model uncertainty. A repetition of the three-transponder measurement campaign should address the multipath issues in more detail.

The multipath model error affects all three measurements simultaneously, which is why this uncertainty was not included in Section 4.3.1. Nevertheless, it is also scaled by the sensitivity coefficient c_P derived previously.

Uncertainties due to external attenuators.   Additional fixed attenuators were integrated into the signal path of each transponder just before the transmitting antenna. Opening and closing of coaxial connectors, and the limited knowledge of the attenuators' attenuation D result in uncertainties for the final RCS.

The overall standard uncertainty arising from using additional fixed attenuators is assessed to be 0.02 dB. This value was derived by measuring the fixed attenuation in C-band with three different network analyzers and three different network analyzer calibration kits. Opening and closing of coaxial connectors was automatically included as part of the measurement procedure.

Distance measurements.   The sensitivity coefficient c_R of the transponder RCS on measurements of the transponder-to-transponder distance R follows from

$$c_R = \frac{\partial \varsigma}{\partial R} = \frac{20}{\ln(10)R} = 8.87R^{-1}. \tag{20}$$

At $R = 46\,\mathrm{m}$ ($z = 0\,\mathrm{cm}$), this results in $c_R = 0.193$. For larger values of R, i.e., for $z > 0\,\mathrm{m}$, c_R decreases so that the value at $R = 46\,\mathrm{m}$ can be taken as the worst-case figure.

The main uncertainty in determining R is not seen in the tachymeter measurement, which can be completed with a standard uncertainty of much below 1 cm. The main contribution rather stems from

---

[¶] The value in decibel is equivalent to an amplitude difference of 23 DA at a reference amplitude of 282 DA.

the insufficient knowledge of the location of the horn antenna phase centers. For this analysis, a standard uncertainty of 20 cm is assumed. The radiometric uncertainty then results from a multiplication of the sensitivity coefficient with this value, giving a relative standard uncertainty of 0.04 dB.

Vector antenna measurements could help in more accurately determining the antenna phase centers through measurements in the future.

4.3.3. Resulting RCS Estimates and Combined Standard Uncertainty

The previously derived uncertainties are now joined using Eq. (18) to yield the final combined standard RCS uncertainty of 0.38 dB. An overview of the top-level uncertainty contributions is given in Table 5.

Table 5. Overview of top-level contributions to the combined standard uncertainty $u_c(\varsigma)$ of transponder RCS's derived during the first demonstration of the three-transponder method.

Uncertainty contribution	$u(x_i)$	c_i	$c_i u(x_i)$ [dB]
Multipath model error	0.75 dB	0.5	0.375
Measurement of distance R	0.2 m	$0.19\,\mathrm{m}^{-1}$	0.039
Estimate of P_{AB}	0.07 dB	0.5	0.036
Estimate of P_{AC}	0.07 dB	0.5	0.036
Estimate of P_{BC}	0.07 dB	0.5	0.036
External attenuator D	0.02 dB	1	0.02
Resulting combined standard uncertainty in dB			0.38

The combined standard uncertainties together with the best RCS estimates from Section 4.2 form the final measurement results, summarized in Table 6. Here the best estimate is taken from the sweep triplet where absorbers were used, as the model (14) seems to more reasonably fit the data (see Fig. 7) so that the results seem more credible.

Table 6. Final measurement results of the three-transponder method demonstration campaign. The RCS estimates are taken from Table 3 for the sweep triplet using absorbers. The 95% confidence intervals (CIs) are derived from the combined standard uncertainty from Table 5 and are therefore considerably wider than the intervals reported in Table 3 for the intermediate results.

Transponder	ς [dBm^2]	95% CI [dBm^2]
Device A (Kalibri 2)	66.28	$[65.5; 67.0]$
Device B (Kalibri 3)	66.10	$[65.3; 66.9]$
Device C (Kalibri 1)	66.04	$[65.3; 66.8]$

In summary it can be concluded that all three measured DLR C-band transponders have a co-polar RCS of slightly above 66 dBm^2, or equivalently, an RCS of slightly above 60 dBm^2 when the transponders are operated in the nominal 45° configuration, fulfilling the transponder requirements.

Furthermore, the measurement results were shown to be compatible (within a confidence level of 95%) with the results of two other independent transponder calibration campaigns. These results are documented in [20].

4.4. Discussion of Measurement Results

Overall, the three-transponder method demonstration measurement campaign can be considered a success. The method allowed for the first time to derive the transponder RCS's of three transponders in an end-to-end configuration without the need for additional RCS calibration targets.

Further principal confidence in the results can be drawn from a comparison of the derived frequency dependent RCS with the transponder frequency response measured (without antennas) in the laboratory with a network analyzer, see Fig. 8. The drop of the measured transmission with respect to the RCS for higher frequencies is partly explained by the frequency dependence of the antenna gains. Between the lower and upper frequencies of the transponder band, ranging from 5.355 GHz to 5.455 GHz, an RCS difference of

$$20 \log \left(\frac{5.455 \,\text{GHz}}{5.355 \,\text{GHz}} \right) = 0.16 \,\text{dB}$$

is expected alone because of the principal antenna gain dependence on frequency. Although this value does not exclusively explain the difference between the three-transponder method and NWA curves, the sign and the general trend is certainly correct.

Despite the encouraging findings for this first demonstration campaign, the derived combined RCS standard uncertainty of 0.38 dB is rather large in comparison to other measurement methods (e.g., 0.2 dB for measurements with corner reflectors (main uncertainty contributors) exploiting satellite overpasses, see [5]). Yet there is no reason in ascribing the uncertainty to the three-transponder method itself. The comparatively large measurement uncertainty is rather attributed to the ad hoc demonstration measurement setup and the multipath contributions. Consequently, the following steps can be taken to improve the accuracy of future three-transponder method measurements:

- Ensure a better suppression of multipath signals, e.g., by installing absorbers with a higher reflection loss on all relevant reflection areas.
- Increase the vertical separation between transponders and ground (or ledges). This results in steeper angles for the multipath signal at the transponder antenna, which results in a higher frequency of the observed standing wave. Consequently, the multipath amplitude can more easily be estimated or simply averaged out even if the maximum traversing range of the slide is only about 1 m.
- Use a slide with a larger maximum traversing range. Again, this helps to capture more periods of the standing-wave pattern so that a more accurate estimation of multipath parameters becomes possible.

Should these measures lead to a suppression of the modeling error of 0.75 dB in Table 5, a total RCS uncertainty of only 0.08 dB would result.

In summary, the three-transponder method promises to deliver transponder RCS measurements with unprecedented low measurement uncertainties in the future, as the main source of measurement uncertainties, the calibration RCS target, could be excluded from the uncertainty budget.

5. DISCUSSIONS OF THE THREE-TRANSPONDER METHOD

5.1. Advantages

These are the reasons which might render the three-transponder method advantageous in comparison to the existing transponder RCS measurment methods discussed in Section 2:

(i) The transponder RCS's can be determined without the need of an additional (passive) radar target with known RCS. By avoiding a comparative RCS measurement, uncertainties resulting from the RCS measurement standard are eliminated.

(ii) The transponders' RX and TX paths are measured in their final configuration. No additional uncertainties result from reassembling cabling after the end of the measurement campaign (assuming an appropriate far-field distance). Also, problems like mismatches between generator and antenna or antenna and receiver need to be handled separately in the three-antenna method; in the three-transponder method, mismatches are also part of the final system and are directly reflected in the measurement results.

(iii) The method allows to determine the transponder RCS at different polarization settings. This is achieved by rotating the transponder antennas and repeating the measurements for each new configuration. Alternatively, if the antenna rotation is precisely known, it can be derived analytically from a set of measurements at one polarization setting.

(iv) No additional RF measurement instrument is needed to complete the measurements. This might help in reducing the costs of a measurement campaign.

(v) The three-antenna measurement technique is well established. A lot of experience exist in the metrology community (e.g., with respect to multipath suppression), which can directly be carried over to the three-transponder measurement method.

(vi) The transponders which are operated as radar targets can easily implement a (digital) delay between receive and transmit. This results in a decoupling of reception and transmission in the time domain. Effectively, the transponder is not operated in a "closed-loop" anymore with respect to erroneous reflections, so that unwanted oscillations, which were observed during previous measurement campaigns in an anechoic chamber, are impossible. Also, the background RCS (e.g., from a tower on which the transponder is mounted, or the back wall in an anechoic chamber) has no effect on the derived transponder RCS when the radar transmit and receive windows are separated in time.

5.2. Limitations

The main limitations of the novel method are:

(i) More than one transponder is needed for a single measurement campaign. Transponders cannot be measured separately according to the proposed method.

(ii) At least one transponder needs to be designed according to Fig. 2, i.e., the transponder must allow operation as a radar and as a transponder instrument. It is sufficient if one of the transponders is replaced by a passive target with an unknown but constant RCS though (see Eq. (11), where device C is only operated as a radar target, not as a transponder).

(iii) The transmit and receive power cannot be freely chosen as for the three-antenna method. Rather, the transponder transmit power is determined by the transponder RCS and a maximal transponder input power (depending on the SAR system the transponder was designed for). To complete the three-transponder measurements, the free-space path loss (and therefore the distance R between the devices) needs to be adjusted so that the measurements can be performed within the operational range of the transponder. Alternatively, the operational range can be adapted by additional stable attenuators.

6. CONCLUSIONS

This paper introduced a novel measurement method for the accurate calibration of a transponder's frequency-dependent RCS. As a derivative of the three-antenna method, an RCS measurement method was introduced which does not depend on additional radar reference targets, while still performing an end-to-end calibration. The soundness of the novel three-transponder method was demonstrated through a measurement campaign for DLR's three *Kalibri* C-band transponders, leading to measurement results after uncertainty analysis which are compatible with two further independent measurement campaigns.

The three-transponder method promises to become one of the, if not the most accurate method for calibrating the RCS of transponders in the future, and it is therefore contributing to radiometrically more accurate SAR systems.

REFERENCES

1. Brunfeldt, D. R. and F. T. Ulaby, "Active reflector for radar calibration," *IEEE Transactions on Geoscience and Remote Sensing*, Vol. GE-22, No. 2, 165–169, Mar. 1984.

2. Curlander, J. C., *Synthetic Aperture Radar: Systems and Signal Processing*, John Wiley & Sons, Inc., 1991.

3. Döring, B. J. and M. Schwerdt, "The radiometric measurement quantity for SAR images," *IEEE Transactions on Geoscience and Remote Sensing*, Vol. 51, No. 12, 5307–5314, Feb. 2013.

4. Döring, B. J., et al., Absolute radiometric calibration of TerraSAR-X — Approach and ground targets," *Microwave Conference (GeMIC)*, 55–58, VDE, 2008.

5. Döring, B. J., et al., "Hierarchical Bayesian data analysis in radiometric SAR system calibration: A case study on transponder calibration with RADARSAT-2 data," *Remote Sensing*, Vol. 12, No. 5, 6667–6690, 2013.

6. Döring, B. J., et al., "Highly accurate calibration target for multiple mode SAR systems," *8th European Conference on Synthetic Aperture Radar*, 1–4, Jun. 2010.

7. Döring, B. J., et al., "Reference target correction based on point target SAR simulation," *IEEE Transactions on Geoscience and Remote Sensing*, Vol. 50, No. 3, 951–959, Mar. 2012.

8. Foged, L. J., M. Sierra-Castaner, and L. Scialacqua, "Facility comparison campaigns within EurAAP," *EUCAP Conference*, IEEE, 2011.

9. Freeman, A., "SAR calibration: An overview," *IEEE Transactions on Geoscience and Remote Sensing*, Vol. 30, No. 6, 1107–1121, Nov. 1992.

10. Gelman, A., et al., *Bayesian Data Analysis*, 3rd Edition, Chapman & Hall/CRC, Boca Raton, 2013.

11. "Evaluation of measurement data — Guide to the expression of uncertainty in measurement," *ISO/IEC Guide 98-3:2008*, Nor. 2008.

12. Jackson, H. D. and A. Woode, "Development of the ERS-1 active radar calibration unit," *IEEE Transactions on Microwave Theory and Techniques*, Vol. 40, No. 6, 1063–1069, Jun. 1992.

13. Jirousek, M., et al., "Development of the highly accurate DLR Kalibri transponder," *Proceedings of 10th European Conference on Sythetic Aperture Radar*, 1–4, 2014.

14. Knott, E. F., J. F. Shaeffer, and M. T. Tuley, *Radar Cross Section*, 2nd Edition, SciTech Publishing, Raleigh, NC, 2004.

15. Kummer, W. H. and E. S. Gillespie, "Antenna measurements — 1978," *Proceedings of the IEEE*, Vol. 66, No. 4, 483–507, Apr. 1978.

16. Raab, S., "Planung und Durchführung einer Freifeld-RCS-Messreihe zur genauen Kalibrierung von Referenzzielen," MA Thesis, Hochschule für angewandte Wissenschaften Würzburg-Schweinfurt, 2013.

17. Raab, S., "Transponderausrichtung bei der Drei-Transponder-Methode: Anleitung und Protokoll zur Kampagne im Dezember 2013," Tech. Rep., Issue 1.0, DLR (German Aerospace Center), Jan. 2014.

18. Raab, S., et al., "Comparison of absolute radiometric transponder calibration strategies," *Proceedings of the European Conference on Synthetic Aperture Radar*, 1–4, 2014.

19. Ross, S. M., *Statistik für Ingenieure und Naturwissenschaftler*, 3rd Edition, Spektrum Akademischer Verlag, 2006.

20. Rudolf, D., et al., "Absolute radiometric calibration of C-band transponders with proven plausibility," *Proceedings of the European Conference on Sythetic Aperture Radar*, 2014.

21. Schwerdt, M., et al., "Final TerraSAR-X calibration results based on novel efficient methods," *IEEE Transactions on Geoscience and Remote Sensing*, Vol. 48, No. 2, 677–689, Feb. 2010.

22. Schwerdt, M., et al, "Independent Verification of the Sentinel-1A system calibration: First results," *Proceedings of the European Conference on Synthetic Aperture Radar*, 1259–1262, VDE Verlag GmbH, Berlin, 2014.

23. Warren, L., *Stutzmann and Gary A. Thiele. Antenna Theory and Design*, 2nd Edition, John Wiley & Sons, Inc., 1998.